

Structure of rutile TiO_2 (1 1 0) in water and 1 molal Rb^+ at pH 12: Inter-relationship among surface charge, interfacial hydration structure, and substrate structural displacements [☆]

Zhan Zhang ^{a,*}, Paul Fenter ^a, Neil C. Sturchio ^b, Michael J. Bedzyk ^{a,c},
Michael L. Machesky ^d, David J. Wesolowski ^e

^a Argonne National Laboratory, CHM, Argonne, IL 60439, USA

^b University of Illinois at Chicago, Chicago, IL, USA

^c Northwestern University, Evanston, IL, USA

^d Illinois State Water Survey, Champaign, IL, USA

^e Oak Ridge National Laboratory, Oak Ridge, TN, USA

Received 18 September 2006; accepted for publication 4 December 2006

Available online 3 January 2007

Abstract

The rutile (1 1 0)–aqueous solution interface structure was measured in deionized water (DIW) and 1 molal (*m*) $\text{RbCl} + \text{RbOH}$ solution (pH 12) at 25 °C with the X-ray crystal truncation rod method. The rutile surface in both solutions consists of a stoichiometric (1 × 1) surface unit mesh with the surface terminated by bridging oxygen (BO) and terminal oxygen (TO) sites, with a mixture of water molecules and hydroxyl groups (OH^-) occupying the TO sites. An additional hydration layer is observed above the TO site, with three distinct water adsorption sites each having well-defined vertical and lateral locations. Rb^+ specifically adsorbs at the tetradentate site between the TO and BO sites, replacing one of the adsorbed water molecules at the interface. There is no further ordered water structure observed above the hydration layer. Structural displacements of atoms at the oxide surface are sensitive to the solution composition. Ti atom displacements from their bulk lattice positions, as large as 0.05 Å at the rutile (1 1 0)–DIW interface, decay in magnitude into the crystal with significant relaxations that are observable down to the fourth Ti-layer below the surface. A systematic outward shift was observed for Ti atom locations below the BO rows, while a systematic inward displacement was found for Ti atoms below the TO rows. The Ti displacements were mostly reduced in contact with the RbCl solution at pH 12, with no statistically significant relaxations in the fourth layer Ti atoms. The distance between the surface 5-fold Ti atoms and the oxygen atoms of the TO site is 2.13 ± 0.03 Å in DIW and 2.05 ± 0.03 Å in the Rb^+ solution, suggesting molecular adsorption of water at the TO site to the rutile (1 1 0) surface in DIW, while at pH 12, adsorption at the TO site is primarily in the form of an adsorbed hydroxyl group.

© 2007 Published by Elsevier B.V.

Keywords: Oxide–water interface; Electrical double layer; Adsorption; Titanium oxide (Rutile); Single crystal surface; X-ray reflection; Surface structure

1. Introduction

When an oxide mineral comes in contact with an aqueous solution, an electrical double layer (EDL) is formed

due to the valence undersaturation of surface atoms resulting in a distribution of water molecules and aqueous ions at the solid–electrolyte interface that is different from either bulk phase [1,2]. The vast majority of studies concerning EDL phenomena implicitly assume that the oxide surface structure is unaffected by the development of an EDL. The oxide–aqueous interfacial structure at the molecular-scale, however, includes the relaxation and/or reconstruction of the oxide surface, the position and the occupation

[☆] Work performed under the auspices of the Office of Science, Division of Chemical Science, US-DOE under contract number DE-AC02-06CH11357.

* Corresponding author. Tel.: +1 630 252 0863; fax: +1 630 252 0862.
E-mail address: zhanzhang@anl.gov (Z. Zhang).

of adsorbed ions, and the arrangement of the water molecules adjacent to the interface. These are all key elements of the EDL, and therefore may be central to a fundamental understanding of ion adsorption, dissolution/precipitation rates and mechanisms, heterogeneous catalysis and other EDL-related phenomena.

The (110) surface of rutile (α -TiO₂) has been studied extensively in the past because of its many applications [3,4]. Many of these applications, such as photo-catalysis and other novel phenomena including photon-induced hydrophilic–hydrophobic transition [5,6] occur in aqueous environments. Most of the work to date concerning the interaction of water with rutile surfaces has involved experimental and theoretical studies of a few water layers adsorbed to rutile. Previous experimental studies yielded information about the surface properties and the water adsorption paths [7–9] under partial vacuum. In particular, comparison of computational and experimental studies in ultra-high vacuum (UHV) prepared surfaces exposed to water vapor led to an apparent contradiction concerning the nature of the adsorbed water, i.e., whether it adsorbs associatively or dissociatively. Most recent studies appear to agree that the first monolayer of water adsorbs associatively on the terrace sites [8,10,11], whereas the dissociation occurs primarily at the bridging oxygen (BO) vacancy sites [7].

There has been discussion concerning the number of Ti-layers needed in the density functional theory (DFT) calculations to approximate a semi-infinite rutile (110) surface structure [10]. It has also been suggested that the addition of the water molecules to the hydrated surface might induce changes in the first hydration layer structure [12]. Therefore, the experimentally measured interfacial structures, including the bulk atom relaxations, the adsorbate locations and coverages, would be a very useful reference in achieving the best model describing the rutile (110)–aqueous interface.

Recent studies have shown that the non-reconstructed TiO₂ (110) (1 × 1) surface is the most stable phase in the O₂ rich (>10^{−4} Torr partial pressure) or humid/aqueous environment [13]. Crystal truncation rod (CTR) measurements of TiO₂ (110) surface in ultra-high vacuum revealed that the surface is terminated with alternative rows of bridging oxygens (BO) bonded to two underlying 6-fold coordinated Ti atoms, 3-fold coordinated oxygen atoms in the Ti–O plane and 5-fold coordinated Ti atoms, with structural displacements as large as 0.27 Å for the top Ti–O tri-layer atoms [14]. A more recent low energy electron diffraction (LEED) measurement found a detailed surface structure that was different from the CTR results but with the similar relaxation amplitudes [15]. Those large interfacial relaxations derive from the truncation of the bulk crystal and in particular the minimization of the energy of the broken bonds associated with the reduced coordination environment of the surface Ti atoms.

The rutile (110) surface structure in contact with aqueous solutions, either pure deionized water (DIW) or in elec-

trolyte solutions containing mono-, di-, and tri-valent cations, has been studied only recently with techniques ranging from X-ray standing waves (XSW), X-ray crystal truncation rod (CTR) measurements, extended X-ray absorption fine structure (EXAFS) spectroscopy, quantum mechanical calculations, classical molecular dynamics simulations, surface complexation models, and pH titrations of powder suspensions and electrophoresis. These studies have provided new insights into EDL phenomena by directly linking microscopic information to macroscopic properties [11,16–27]. In a previous study, a preliminary CTR measurement determined the termination of the rutile surface and found that the surface relaxations are minimal due to the presence of a fully-occupied terminal oxygen (TO) site above the 5-fold Ti surface atom, occupied by either an adsorbed water molecule or a hydroxyl group (OH[−]). The presence of an additional adsorption layer above the TO and BO sites at both the rutile–deionized water (DIW) and rutile–RbCl solution interface was observed at laterally and vertically well-defined locations, with the primary adsorption site located at the tetradentate site between BO and TO sites [23]. The precise surface atom locations and interfacial bond lengths were not, however, determined due to the incomplete data set that was available at that time. A similar study of RuO₂ (110) surface (also having the rutile crystal structure) in aqueous solutions shows behavior very similar to that found for rutile, with the surface Ru oxygen coordination shell completed by an adsorbed water molecule (or hydroxyl group) [28]. More generally, these results indicate that the structures of the oxide surface are significantly different in vacuum and in contact with an aqueous solution.

Here, we report a complete CTR analysis of the rutile (110) surface in contact with DIW and with 1 molal (*m*) RbCl + RbOH at pH 12, revealing the precise interfacial structures under both solution conditions, and the changes associated with interfacial charging and ion adsorption.

2. Materials and methods

2.1. Rutile (110) surface

Rutile (α -TiO₂) has tetragonal structure, with lattice parameters $a_0 = b_0 = 4.5942$ Å, and $c_0 = 2.9587$ Å at $T = 298$ K [3,29]. A non-primitive surface unit cell is defined with its lattice vectors along the crystallographic directions [110], [001], and [110], respectively, as shown in Fig. 1a. The non-primitive unit cell lattice parameters are $\mathbf{a} = \mathbf{c} = \sqrt{2}\mathbf{a}_0 = 6.4972$ Å, and $b = c_0 = 2.9587$ Å. The coordinate system is defined with the origin ($x = y = z = 0$) located on the surface Ti–O plane directly underneath the bridging oxygen (BO) site of an unrelaxed bulk lattice, as shown in Fig. 1. The rectangular unit shown in Fig. 1b is defined as the rutile (110) surface 2D unit cell, with an area of $6.497 \times 2.959 = 19.22$ Å².

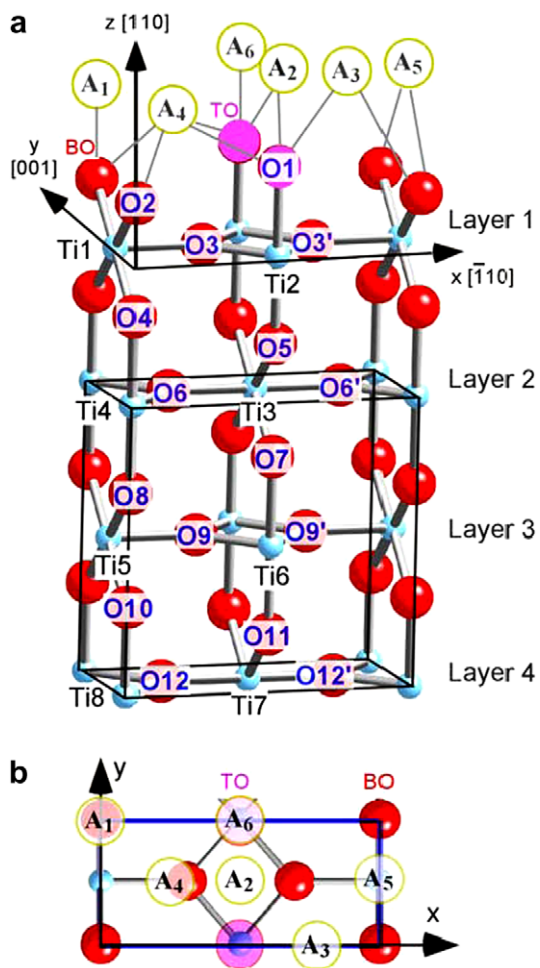


Fig. 1. (a) The ball-and-stick model of rutile TiO_2 (110) surface. Atoms and adsorption sites are labeled as O1–O12, Ti1–Ti8, and A1–A6 for oxygen, titanium, and the adsorbates, respectively. Note that the O2 and O1 sites also referred to as the BO and TO sites, as indicated. The surface non-primitive unit cell and the coordinate axes are shown in the figure, too. Ti–O tri-layers are labeled as Layer 1–4, starting from the surface. (b) A top view of the rutile (110) surface with the lateral locations of the potential adsorption sites.

There are six possible high-symmetry adsorption sites for adsorbed species at the rutile (110)–aqueous interface [26]. These adsorption sites (A_n , $n = 1–6$, as labeled in Fig. 1) are characterized by their lateral positions: A_1 is above the BO site (i.e., monodentate); A_2 is between two terminal oxygen (TO) sites (i.e., bidentate); A_3 is bidentate to one BO and one TO site; A_4 is tetradentate to two BO and two TO sites; A_5 is bidentate between two BO sites; and A_6 is monodentate to one TO site.

The rutile bulk Bragg peaks and the surface truncation rods are shown in a reciprocal space representation (Fig. 2). Only one quadrant of the reciprocal space above the surface is shown. The other three quadrants can be achieved based on the rutile (110) surface symmetry (having two orthogonal mirror planes perpendicular to the surface and along the Q_x and Q_y directions, respectively). Dashed vertical lines indicate the weaker “oxygen only”

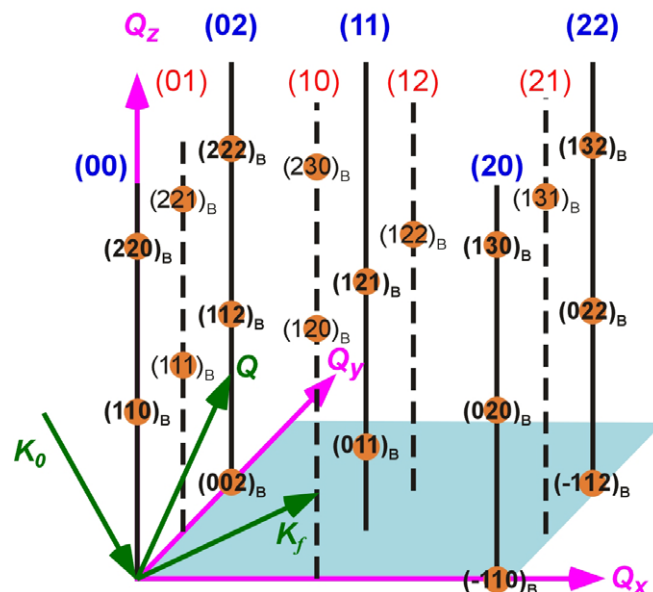


Fig. 2. The reciprocal space representation of the rutile (110) surface including substrate Bragg peak locations and the surface crystal truncation rods. The rutile Bragg peaks are labeled with their traditional bulk notation (subscripted with a ‘B’) and the rods are labeled (at top) with the surface Miller indices (H K). The dashed vertical lines indicate the weaker ‘oxygen only’ rods, where substrate lattice Ti atoms have no contribution for an ideally terminated lattice; the solid vertical lines indicate the strong ‘mixed rods’ with both Ti and O contributions.

rods, where bulk Ti atoms do not contribute to the scattering intensity [28]. The solid vertical lines are the strong rods that have contributions from both lattice Ti and O atoms.

Polished rutile (110) single crystals ($10 \times 10 \times 1 \text{ mm}^3$) were obtained from Princeton Scientific. The sample preparation procedure, resulting in a surface topography with large atomically flat terraces, is described elsewhere [27]. The miscut of the polished TiO_2 crystal surface was found to be $\sim 0.08^\circ$, which translates to an average terrace width between adjacent steps of $\sim 0.21 \text{ m}$ with a step height of 3.25 \AA . Under such condition, the terrace sites are the dominant adsorption sites on the surface.

2.2. Crystal truncation rod method

X-ray crystallography has long been used to determine bulk material structures because the interaction between X-ray and matter can be described quantitatively by kinematical diffraction theory. The CTR measurement is the interfacial analog of bulk crystallography [30]. Interfacial signals appear as continuously modulated rods of intensity extending from each Bragg peak due to the loss of translational invariance associated with the presence of the surface, and are known as crystal truncation rods [30]. The CTR method has been successfully applied to probe the surface structure of oxides and other minerals surface in both vacuum and ambient condition [14,28,31–36] due to its quantitative capability and sub-Ångström resolution.

The measurement can be carried out in situ at the oxide–aqueous interface since X-rays readily penetrate water. Typically, the strength of the CTR signal at the mid-point between Bragg peaks corresponds to one-half of a surface monolayer. On the other hand, the number of adsorbed species (e.g., water, ions) is comparable to one monolayer of the oxide. Therefore, the CTR measurement is expected to be directly sensitive to the oxide–aqueous interfacial structures.

The details of analyzing CTR data for mineral–water interface can be found in the reference [34,36,37]. In brief, the normalized interfacial scattering intensity R_N (after correcting for variations in incident flux, active area, resolution function, and Lorenz factor, etc.) can be written as

$$R_N = S \cdot T_{\text{cell}} \cdot B \cdot |F|^2; \quad (1)$$

where S is an overall scale-factor (due to the normalization of photon counting scintillation detector signals to the charge collecting ion chamber signals); T_{cell} is the angle-dependent X-ray transmission through the bulk water and sample cell window; B is the roughness factor, which is calculated assuming the roughness is in the form of partial layering with the occupancy of n th layer as b^n , where $b(0.6 \leq b \leq 1)$ indicates the fractional occupancy [30]; and F is the structure factor of the oxide–water interface system, which has three components

$$F = F_{\text{bulk}} + F_{\text{inter}} + F_{\text{water}}; \quad (2)$$

Here F_{bulk} is the contribution from the semi-infinite bulk crystal; F_{water} is from the macroscopic water layer above the surface; and F_{inter} is from the interfacial region, including a few top layers of the crystal, which could be relaxed and/or reconstructed, any specifically adsorbed species at the crystal surface, and a few layers of the water molecules next to the interface. The structures of the bulk crystal and bulk water, i.e., F_{bulk} and F_{water} , are known before hand, thus the interfacial structure factor F_{inter} can be determined from the measured reflectivity.

The unknown interfacial structure is solved by model-dependent non-linear χ^2 fitting through direct comparison of measured and calculated interfacial scattering intensities [38,39]. Because the fitting procedure may not always find the global minimum, a reasonable starting structure is critical in model-fitting the CTR data. The best-fit model structure should not only generate calculated structure factors that best match the measure ones, but also be physically and chemically plausible, e.g., the atom packing density and bond lengths should both be chemically reasonable.

3. Experiment details

3.1. CTR measurements

The CTR measurements were performed primarily at beamline 1BM-C at Advanced Photon Source (APS), Argonne National Laboratory (ANL) and preliminary work

was done at beamlines 12BM-B, 11ID-D, and 12ID-D at the APS. At 1BM-C, a symmetrical Si(111) high heat load monochromator is used to select the X-ray energy of ~ 14.8 keV for both $\text{TiO}_2/\text{H}_2\text{O}$ and TiO_2/RbCl solution measurements. The incident beam was focused at the center of the diffractometer horizontally with a sagittal focusing monochromator and vertically with a focusing mirror [40]. The beam size is further reduced by a set of slits to a size of $0.45 \times 0.3 \text{ mm}^2$ (horizontal and vertical, respectively) at the sample surface. The X-ray beam intensity after the incident slit was monitored with an ionized chamber filled with pure dry N_2 gas. A CyberStar[®] scintillation detector was used to record the reflected X-ray beam intensity.

The measurements were performed in-situ in a thin-film cell [41]. The solution exchange procedure was the same as that in the XSW measurements described previously [27]. Before each measurement, the solution between the Kapton film and the sample surface was drained and the cell is sealed to maintain a minimal ($\sim 2 \text{ m}$ thick) solution thickness during the CTR measurements. Solution is occasionally flushed through the cell to maintain the nominal solution condition.

The rutile crystal was mounted initially in deionized ultra-filtered water (DIW, $>18 \text{ MX}$). After the full set of CTR measurements were done for the TiO_2 –DIW interface, 1 molal (m) $\text{RbCl} + \text{RbOH}$ solution (referred to as RbCl solution hereafter) at pH 12 was exchanged into the sample cell and another full set of CTR data was measured. The high solution concentration was selected because previous XSW measurements failed to detect specific adsorption of Rb^+ ions at lower concentrations ($<10^{-3} m$) [23].

Care was taken to find an area on the crystal surface that had a uniform reflectivity near the first mid-zone along the specular reflectivity rod (i.e., $L = 1.1$ reciprocal lattice unit (rlu) on the (00) rod), which is sensitive primarily to the surface structure and roughness. The area has the size $\sim 1 \text{ mm}$ larger than the beam footprint both along and transverse to the X-ray beam directions. Under such condition, even if there were relative motions of the X-ray beam over the sample surface during the measurements (e.g., caused by a minor misalignment or temperature change inside the hutch), all of the measured CTR data can be associated with a single unique interface structure.

Fiducial points were monitored frequently throughout the measurement. Both bulk and surface sensitive fiducials (e.g., $L = 1.9$ and 1.1 rlu on the (00) rod, respectively) were measured repeatedly. The observed constant reflectivity at all fiducial points ensured the surface was stable during the measurement. Surface symmetry equivalent rods were checked by measuring (11) rod equivalents, i.e., (11), (11), (11), and (11) rods. Both bulk dominant ($L = 2.9$ and $L = 1.2$) and surface sensitive signals ($L = 2.1$ and $L = 3.7$) were measured on each rod. The small variation of measured reflectivity from rod to rod indicates that systematic error for the non-specular crystal truncation rod measurements was small ($<10\%$) and the measured reflectivity

tivity modulation on the rod was determined by the intrinsic interfacial structure, not the extrinsic factors, such as the setup or alignment error.

The CTR measurements were carried out at the same beamline at two different times. During the first measurements, (00), (02), (20), and (11) rods were measured for both rutile–DIW and rutile–RbCl solution interfaces and (40) rod was also measured for rutile–RbCl solution interface. For the second set of the measurements, (00), (10), (01), (12), and (21) rods were measured under both solution conditions and (20) was measured in addition for rutile–RbCl solution interface. The setup was identical for both runs to minimize the effects of the extrinsic factors, such as the slit settings and the detector to sample distance. A total of 531 and 689 unique reflections were measured for rutile (110) surface in DIW and in RbCl solution, respectively.

The CTR data were measured in the symmetric scattering mode by rocking the spectrometer angle θ (i.e., within the vertical scattering plane) at each vertical momentum transfer Q_z value on a specific rod. For each rocking scan, the background subtracted integrated intensity was obtained as the raw reflectivity. Geometry related corrections were applied to the raw reflectivity, including the active area correction, resolution function correction, and Lorentz factor, etc., [34]. The corrected interfacial scattering intensity as a function of Q_z is plotted in Fig. 3.

The statistical uncertainties for the measured reflectivity were very small (<1%) except for a few points. However, to account for the (possible) systematic errors described above, a minimum uncertainty of 10% was imposed on all data points.

3.2. Data analysis

For the rutile–DIW interface, the (00) rods measured at different times overlap very well, indicating that the extrinsic factors are accounted for properly and the interfacial structures are identical. For the rutile–RbCl solution interface, however, the repeated measurements of (00) and (20) rods show differences, which appears to be primarily due to the difference in the Rb^+ occupancy factors between the two measurements.

According to the theoretical calculations and ultra-high vacuum based measurements, the TiO_2 (110) surface in DIW at room temperature and one atmosphere pressure should not be reconstructed [13,42,43]. Therefore the single non-primitive unit cell shown in Fig. 1 is used as the basic structural unit. The bulk crystal is obtained by semi-infinitely repeating the unit. Atom positions in the bulk are held fixed in the analysis.

The bulk solution can be modeled in two different ways, either as a structureless error function profile or as a layered fluid. For the layered water model, the density is modeled with a series of Gaussian functions extending from the interface into the bulk solution with a fixed spacing but an increasing width as the distance from the interface in-

creases [34,36,44,45]. The structureless water model follows an error function profile that is treated as a continuous medium with an electron density of $0.33 \text{ e}^-/\text{\AA}^3$. The use of a layered water model with its additional detail and structural parameters did not improve the fitting quality. Therefore only the simpler structureless water model is used and discussed. The parameter that defines the thickness of the water layer includes the actual water and the 81 m-thick plastic (Kapton) window because the densities of the plastic and water are very similar and this approximation simplifies the calculation.

The interface region includes vertically two non-primitive unit cells (i.e. 4 Ti-layers) and adsorbates at the rutile–water interface, as shown in Fig. 1a. The nominal high-symmetry sites are labeled for oxygen (O_n), titanium (Ti_n) and adsorbate (A_n), respectively, with n the index indicated at each site.

The structural model primarily includes the offsets of the interfacial atoms from their lattice positions and their occupancy factors, as listed in Table 1. For instance, the z -direction offsets for all the atoms in the top layers (O1–O8 and Ti1–Ti8 in Fig. 1a) from their bulk lattice positions are included; lateral offsets of the atoms in the top Ti-layer are also included, e.g., based on the rutile (110) surface symmetry, O3 and O1 (BO) have offsets along x -direction, but not along y -direction. In order to substantially reduce the number of independent structural parameters, the z -direction offsets for O9–O12 are not directly parameterized; instead, they are calculated based on the neighboring Ti positions assuming the coplanar of Ti–O bonds around an O atom. For example, D_z of O9 can be calculated from the positions and the offsets of Ti5 and Ti6: $Dz_{O9} = Dz_{Ti5} \cdot \frac{x_{Ti6} - x_{O9}}{x_{Ti6} - x_{Ti5}} + Dz_{Ti6} \cdot \frac{x_{O9} - x_{Ti5}}{x_{Ti6} - x_{Ti5}}$, where x_n and Dz_n are the x coordinate and z offset of the atom n , respectively. The occupancy factors C for sites O1 and Ti2 and sites O2 and Ti1 are set to be equal (i.e. $C_{O1} = C_{Ti2}$; $C_{O2} = C_{Ti1}$) and allowed to vary. The adsorbates (H_2O and/or Rb^+) are allowed to displace from their initial positions freely and their occupancy factors are fitted. Occupancy factors are reported in the unit of monolayer (ML), where 1 ML is defined as 1 atom/molecule/ion per rutile (110) surface 2D unit cell, i.e. $1 \text{ ML} = 1/(19.22 \text{ \AA}^2) = 8.81 \text{ mol/m}^2$. Adsorbates are primarily located near the A_4 site as indicated by the earlier study [23]. For completeness, combinations of all A_1 – A_6 sites are explored.

The symmetry of rutile (110) surface is assumed in all calculations so that symmetry equivalent atoms have equivalent structural relaxations and occupations. For instance, if O3 moves 0.1 \AA along x -direction, O3' should have an offset of -0.1 \AA from its lattice position. And if TO has a lateral offset of (D_x, D_y) from its lattice site, the occupancy factors are equally distributed between this and the three other symmetry equivalent sites with displacements of $(-D_x, D_y)$, $(D_x, -D_y)$, and $(-D_x, -D_y)$, respectively.

The vibration amplitudes of the bulk atoms and adsorbate are included for calculating the Debye–Waller factor. The vibration amplitudes along the three primary axes for

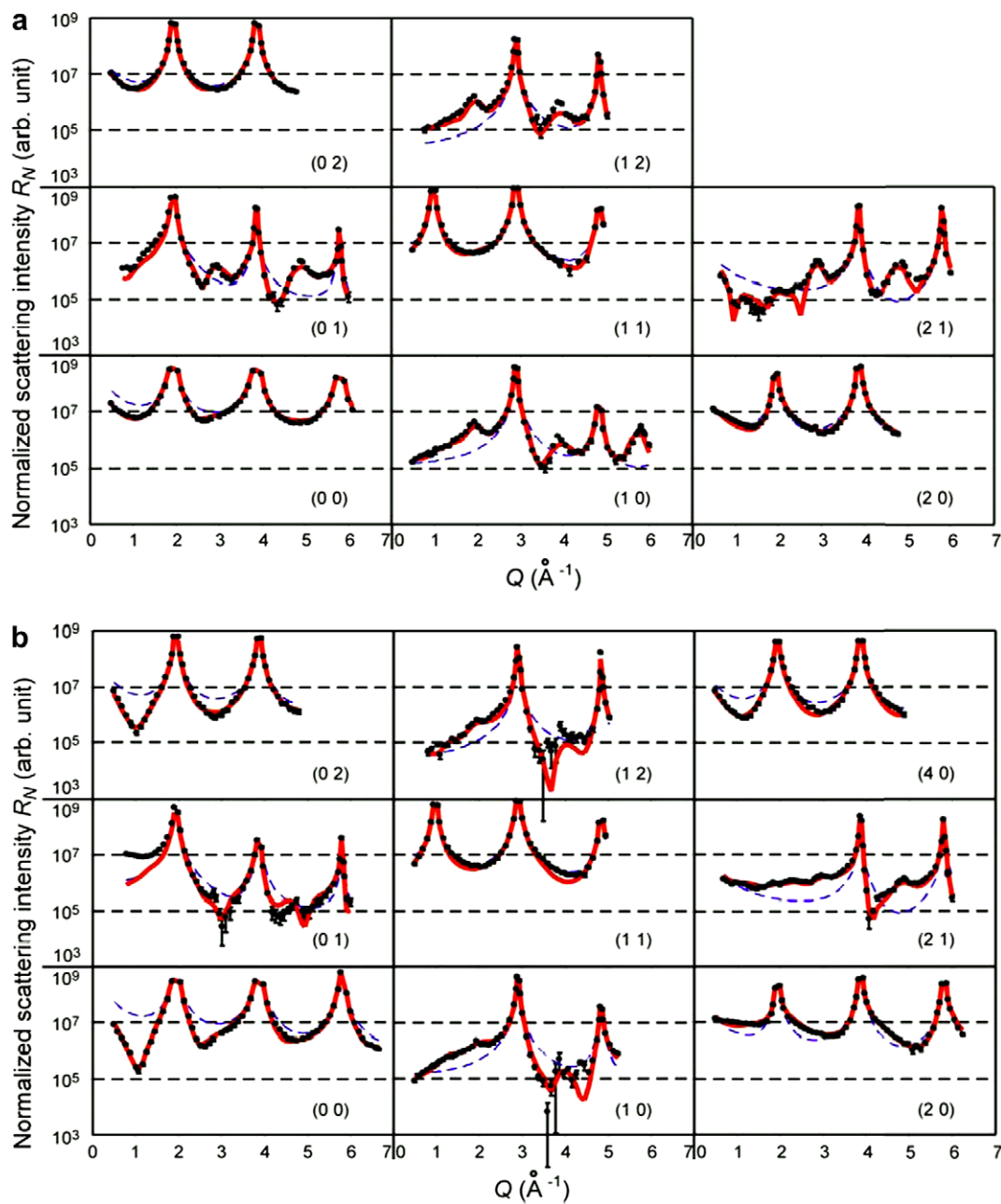


Fig. 3. The measured normalized scattering intensities (points with errorbars) and calculations based on the best fit structures (solid line) for rutile (110) surface in (a) DIW and (b) pH 12, 1 *m* RbCl solution. Dashed lines are the calculations for an ideally-terminated non-relaxed rutile (110) surface with both BO and TO present.

each atom in rutile crystal are known [46] and included in the calculation. For surface atoms, adsorbates and bulk water molecules, the primary vibration amplitudes can be included as fitting parameters. However, we find that the fitting does not uniquely determine the vibration amplitudes and the occupancy factors simultaneously because they are correlated. The vibration amplitudes have been fixed at reasonable values, e.g., 0.1–0.2 Å for the interface atoms, 0.1–0.3 Å for the adsorbate and ~ 0.3 Å for bulk water molecules, since they are typically smaller than the resolution of the CTR measurements (~ 0.5 Å in this study

along the surface normal direction). These values are varied to check their effects on the respective occupancy factors so that the full uncertainties in the vibration amplitudes are determined.

There are a few fitting parameters that are extrinsic to the interfacial structure, including the overall scale factor, the b-factor to calculate the roughness factor, and the bulk water thickness. Two independent Rb^+ occupancy factors are used for the two sets of rutile–RbCl solution rods due to the small but significant differences in the measured intensities for the two data sets.

Table 1

Offsets from the projected bulk atom sites (in Å), locations of the adsorbates (in Å), and the occupancy factors (in ML) at the rutile (110)–DIW and RbCl solution interface

		Vacuum studies		This study	
		CTR	LEED	In DIW	In RbCl solution
Ti1	D _y	–	–	–	0.04(3)
	D _z	0.12(5)	0.25(3)	–0.002(4)	–0.019(4)
	C	1	–	0.93(1)	0.88(1)
Ti2	D _y	–	–	–	0.07(2)
	D _z	–0.16(5)	–0.19(3)	–0.051(4)	–0.036(4)
	C	1	–	0.95(1)	0.87(1)
Ti3	D _z	–0.09(4)	–0.09(7)	–0.016(4)	0.001(4)
Ti4	D _z	0.07(4)	0.14(5)	0.021(4)	0.006(4)
Ti5	D _z	–	–	0.013(3)	0.009(3)
Ti6	D _z	–	–	–0.010(3)	–0.001(3)
Ti7	D _z	–	–	–0.007(2)	0.001(2)
Ti8	D _z	–	–	0.009(2)	0.004(2)
O1	D _x	–	–	0.00(3)	0.00(2)
	D _z	–	–	0.101(8)	0.029(12)
	C	0	0	0.95(1)	0.87(1)
O2	D _z	–0.27(8)	0.10(5)	0.004(9)	0.010(11)
	C	0.94(5)	–	0.93(1)	0.88(1)
O3	D _x	–0.16(8)	–0.17(15)	–0.09(2)	–0.00(1)
	D _z	0.05(5)	0.27(8)	0.068(6)	0.026(8)
	C	1	–	0.89(3)	0.87(2)
O4	D _z	0.05(8)	0.06(10)	0.008(7)	0.013(9)
O5	D _z	0.00(8)	0.00(8)	–0.012(8)	0.013(9)
O6	D _x	–0.07(6)	–0.07(18)	–0.05(1)	–0.00(1)
	D _z	0.02(6)	0.06(12)	0.015(6)	0.017(6)
O7	D _z	–0.09(8)	0.00(17)	0.005(7)	0.008(8)
O8	D _z	–0.12(7)	0.01(13)	–0.002(7)	0.000(8)
AW1	x	–	–	0.00(4)	0.63(6)
	y	–	–	0.00(1)	0.00(4)
	z	–	–	3.69(2)	3.60(2)
	C	–	–	0.75(4)	0.68(5)
AW2	x	–	–	1.17(3)	2.91(9)
	y	–	–	1.48(3)	1.23(6)
	z	–	–	3.61(2)	4.27(4)
	C	–	–	0.68(9)	0.37(4)
AW3	x	–	–	1.82(6)	2.43(8)
	y	–	–	0.73(7)	1.45(52)
	z	–	–	3.87(10)	5.15(4)
	C	–	–	0.87(12)	0.33(7)
Rb ⁺	x	–	–	–	1.38(2)
	y	–	–	–	1.66(2)
	z	–	–	–	3.44(1)
	C ₁	–	–	–	0.52(2)
	C ₂	–	–	–	0.42(2)
Bulk water	z	–	–	4.90(13)	5.66(10)

AW_n ($n = 1, 2, 3$) represents the adsorbed water molecules; D_x, D_y, and D_z are the offsets of the Ti and O atoms from their bulk lattice positions; x, y, and z are the locations of the adsorbates; C represents the occupancy factor of the interfacial sites; C₁ and C₂ are the Rb⁺ coverages measured at two separate occasions, respectively. For comparison, values from the vacuum studies are listed for CTR and LEED experiments [14,15]. Numbers in the parentheses are the uncertainties for the last one or two digits. ‘–’ indicates the parameter is not included in the model.

4. Results and discussion

4.1. Rutile (110)–DIW interface results

The experimental data are shown in Fig. 3a, with solid lines that represent the calculated reflectivity from the best fit structures and the dashed lines represent the calculation based on the ideally-terminated rutile (110) surface with

both BO and TO sites fully occupied. It is immediately apparent from these data that the ideally terminated surface provides an approximate qualitative explanation of only the rods with surface Miller indices $H + K = \text{even}$, but that substantial discrepancies are found for the oxygen only rods ($H + K = \text{odd}$). In particular, a significant additional oscillation in the experimental data is observed with maxima near the anti-Bragg conditions and whose

magnitude appears to increase with Q_z . This feature, however, is not present in the calculation of the ideally terminated surface, which has a quality of fit, $\chi^2 = 62$ (as compared to an expected value of ~ 1 for a model that explains the data perfectly).

The best fit structure explains nearly all of the fine features present in the experimental data. The best fit structures do not differ significantly with or without the repeated measurements of the (00) rod that were measured separately. Therefore, the best fit values reported here include all of the rods in the fitting, though only one of the (00) rods is shown in Fig. 3a. This best-fit model has a quality of fit of $\chi^2 = 3.9$. A ball-and-stick model corresponding to the best-fit model of the rutile–DIW interface is shown in Fig. 4a and b. The laterally averaged electron density, broadened to account for the vertical resolution of the data, is shown in Fig. 5. It is apparent from this plot that the derived structure is consistent with that reported previously based solely on the $H + K = \text{even}$ rods [23].

The best-fit parameters are listed in Table 1 along with the values determined for the rutile (110) surface in ultra-high vacuum. Before we discuss the detailed structural results, it is first necessary to discuss the role of extrinsic parameters. The b-factor from the fitting is 0.00 ± 0.01 , which indicates the sample spot where the measurements were done has virtually no roughness. The measured CTR data are relatively insensitive to the total water layer thickness, with a best fit value of 0 ± 10 Å, whose contribution is primarily at small vertical momentum transfer (i.e. small angles of incidence) where few data points were measured. The order of magnitude of the water layer thickness, though, agrees with the previous estimations [27], i.e., 8-Å-thick Kapton film plus a 2-Å-thick water layer, which also indicates the sample environments were well under control during the X-ray measurements. The total thickness of material above the surface was fixed at 10 Å. Consequently, these extrinsic factors do not contribute significantly to the best-fit structure.

The derived substrate atom displacements from their bulk lattice positions are all significantly smaller when compared to the vacuum studies [8,14,15]. Specifically,

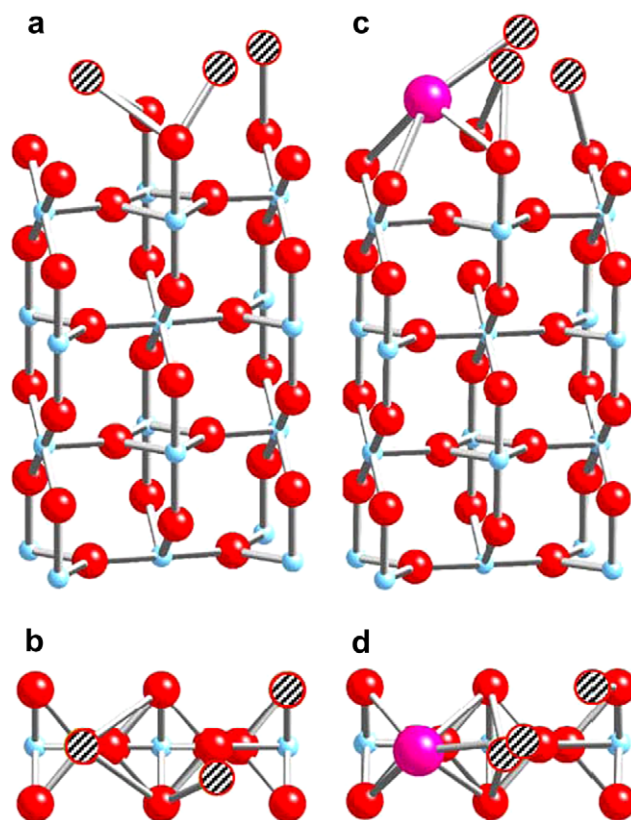


Fig. 4. A ball-and-stick model of the best-fit rutile (110)-aqueous solution interfaces. (a) Perspective and (b) top views of the interface in DIW. (c) Perspective and (d) top view of the interface in RbCl solution. The small (cyan), medium (red), large (pink) spheres, and hatched circles represent Ti, O, Rb⁺, and H₂O, respectively. (For interpretation of the references to colour in this figure legend, the reader is referred to the web version of this article.)

the largest amplitude of Ti atom z -offsets ($Ti2_z$) is only 0.05 Å. The offset amplitudes decay to ~ 0.01 Å at the fourth Ti-layers. Though small, these Ti offsets are critical to reproduce the oscillations between the Bragg peaks on the ‘oxygen only’ rods. For instance, inclusion of relaxations in only the top two layers results in a quality of fit of $\chi^2 \sim 6$ and failed to reproduce the magnitude of the intensity oscillations along the oxygen only rods, indicating

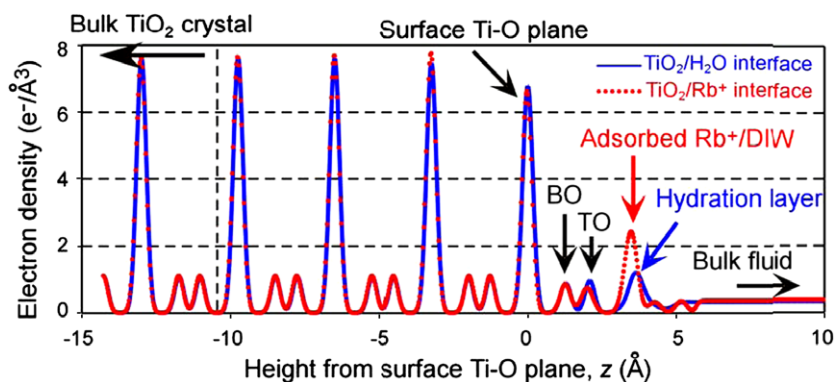


Fig. 5. Laterally averaged electron density profile for rutile (110) surface in DIW and RbCl solution. The increase of the electron density above the TO site in 1 M RbCl solution indicates the specific adsorption of Rb⁺ ions, displacing the water molecules that are specifically adsorbed in DIW.

that deeper layer relaxations are required by the data. Although the surface Ti atoms would have no contribution to the ‘oxygen only’ rods if they were located exactly on their ideal bulk lattice positions, any offset will lead to additional modulation(s) on these rods making the ‘oxygen only’ rods very sensitive to the surface Ti positions. The O atoms in the surface layers, on the other hand, undergo relatively smaller offsets along the z -direction. Around the third Ti-layer, i.e., at sites O7 and O8, the O offsets are essentially zero within uncertainties.

An interesting feature of this structure is found in the offset direction of the near-surface Ti atoms. In particular, almost all of the Ti atoms in the same y - z plane (i.e., under either the BO or TO rows) have the same offset direction, with the sole exception being the Ti1 site. That is, the Ti2, Ti3, Ti6, and Ti7 are all relaxed inward, while Ti4, Ti5, and Ti8 all have an outward relaxation, as shown in Fig. 6. This phenomenon has been observed previously for rutile in vacuum, although those results included only two Ti layers [14,15]. More generally, while there is a change in direction of the Ti1 with respect to the other sites, the difference in the vertical displacements for a given layer (i.e., Ti1 $_z$ -Ti2 $_z$ or Ti3 $_z$ -Ti4 $_z$) decays monotonically into the crystal. This can be interpreted as a propagation of the top layer Ti buckling through the Ti–O–Ti chains into the crystal.

The adsorbed water molecules (above the TO and BO sites) occupy three distinct sites, primarily near the A_1 , A_4 , and A_3 sites, as labeled AW1, AW2, and AW3 in Table 1, respectively, i.e., the adsorbates tend to fill in the channel between the BO and TO rows or lie above the BO rows. This picture is similar to the calculation results of multi-layer water molecules adsorbed at rutile (110) surface [43]. In such an arrangement, the interfacial water molecules could easily form a hydrogen-bond network with each other and with the surface oxygen atoms, which therefore acts to stabilize the interfacial structure [11]. The total coverage of the water molecules at these positions is around 2 ML, which is consistent with the bulk

water density. Above these adsorbed water molecules, no further structured water layers are observed.

4.2. Rutile (110)–RbCl solution interface results

The calculation based on the best fit structure for rutile in contact with 1 *m* RbCl solution is plotted in Fig. 3b, with only one set of measured (00) and (20) data shown. The ball-and-stick model of the rutile–RbCl solution interface is shown in Fig. 4c and d, and the laterally averaged electron density is shown in Fig. 5. For these data, the b -factor is 0.05 ± 0.01 , which translates into root mean square (rms) height of 6 0.75 Å [30]. The slight difference between this derived b -factor value and that of the rutile–DIW interface suggests that the measurements were done on different areas of the surface. As in the DIW analysis, a fixed solution plus Kapton thickness of 10 μ m is assumed because this parameter is poorly constrained by the data.

The best-fit parameters describing this structure are listed in Table 1, with Ti offsets along z -direction that are reduced with respect to that observed for the rutile–DIW interface (Table 1 and Fig. 6). While Ti-atom offsets in the fourth Ti-layer at the rutile–DIW interface are observable, they are not statistically significant at the rutile–RbCl solution interface. Similarly, all other Ti offsets are smaller compared to those observed at the rutile–DIW interface, with the relaxation directions essentially the same. We also observed that the TO height is lower in the RbCl solution than in DIW. Coupled with the decreased Ti2 site offset, the Ti2–O1 distance is reduced by about 0.1 Å.

A significant increase of electron density near the A_4 sites is observed with respect to that observed at the rutile (110)–DIW interface, which is associated with Rb^+ ions replacing the adsorbed H_2O molecules as concluded previously [23]. The small but significant differences between the two sets of CTR data that were analyzed together resulted in separate occupation factors for the adsorbed Rb^+ of 0.52 ± 0.02 and 0.42 ± 0.02 ML, respectively, showing that while the differences are significant, they remain relatively small. The best-fit structure also reveals that the presence of the Rb^+ ions perturbs the interfacial water distribution. The adsorbed H_2O (AW n , $n = 1$ –3) around the A_1 site (AW1) is displaced only slightly along x -direction. However, the H_2O near the A_4 site (AW2) at the rutile–DIW interface moves towards the A_2 site. The AW2–O1 bond length is about 2.6 Å, which implies a hydrogen bond between the two species. There is also an additional contribution of ordered water molecules further away from the surface above the A_2 site (AW3), which could be water in the Rb^+ hydration shell. No attempt was made to complete the Rb^+ hydration shell with more water molecules in order to limit the number of the fitting parameters.

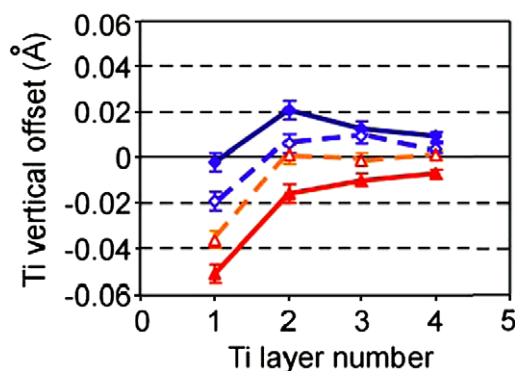


Fig. 6. The vertical offsets of the interfacial Ti atoms as a function of Ti-layer number in DIW (filled symbols and solid line) and in RbCl solution (open symbols and dashed line). Here, the triangles indicate the vertical displacement of Ti atoms below the TO row, while the diamonds indicate the vertical displacement of Ti atoms below the BO row.

5. Discussion

In discussing the present results, we will attempt to provide some perspective related to previous work, which

encompasses both experimental and theoretical studies of rutile interfaces, and for water coverages ranging from sub-monolayer to macroscopic water layers. A surprising aspect of the present results is that the interfacial displacements that we observe penetrate significantly into the bulk crystal (i.e., to at least the fourth Ti-layer in DIW and the third Ti-layer in 1 *m* RbCl solution at pH 12) and that these relaxation patterns and magnitudes are sensitive to the solution conditions. Since the top layer surface relaxations are clearly larger under vacuum conditions, it is reasonable to believe that a similar relaxation pattern would exist in vacuum, perhaps extending even deeper into the bulk crystal. When trying to explain the structural differences between the experimental and theoretical results of the rutile surface relaxation in the vacuum, Thompson and Lewis suggested that the rutile (110) surface relaxation might reach more than 2 Ti-layers deep [47], and an offset as large as 0.1 Å was implied for the third layer and beyond.

The rutile (110) surface relaxations in vacuum are much larger than in DIW, which suggests that the presence of adsorbate substantially relieves the distortion of the crystal at the surface. Specifically, in vacuum where the O1 site is

unoccupied, the Ti2 moves inward and Ti1 moves outward. Accordingly, the Ti atoms in the underlying layers are offset along the same direction with decreasing offsets for deeper layers. The O1 site becomes occupied when the surface is in contact with DIW, presumably by a H₂O molecule, thereby completing the first coordination shell of Ti2 and significantly reducing the inward offset of Ti2. We can expect that the residual Ti2 inward offset in DIW is due to a Ti–OH₂/Ti–OH bond formed between Ti2–O1 that is weaker than the Ti–O bond in the rutile crystal. The vertical displacement of the Ti2 site is even further reduced in the RbCl solution, suggesting that the Ti2–O1 bond becomes stronger either because more OH[−] groups replace H₂O molecules at the O1 site at the elevated pH, or because the adsorption of the Rb⁺ ion has an effect on the bond strength.

Further insight into these issues can be obtained from the derived inter-atomic distances, which are listed in Tables 2 and 3 for the rutile (110) surface in DIW and in RbCl solution, respectively. Most of the Ti–O distances are very close (<3%) to the expected bulk values, with the exception of the Ti2–O1 distance. The derived Ti2–O1 distance for the rutile–DIW interface is 2.13 ± 0.03 Å, which

Table 2

Inter-atomic distances (in Å) for rutile (110)–DIW interface between rutile surface atoms (e.g. Ti1 and O1) and adsorbed water molecules

	AW1	AW2	AW3	Ti1	Ti2	Ti3	Ti4	Ti5	Ti6
O1		2.97(6)	2.37(14)		2.13(3)				
O2	2.42(5)	3.01(5)	3.24(13)	1.95(2)					
O3				1.89(3)	2.01(2)				
O3'					2.01(2)				
O4				1.94(1)			1.97(1)		
O5					1.94(1)	1.95(1)			
O6						2.03(1)	1.91(1)		
O6'						2.03(1)			
O7						1.94(1)			1.99(1)
O8							2.00(1)	1.94(1)	

Numbers in parentheses are the uncertainties for the last one or two digits. Shown in the table are the distances between the adjacent atoms/ions.

Table 3

Inter-atomic distances (in Å) for rutile (110)–RbCl solution interface

	AW1	AW2	AW3	Ti1	Ti2	Ti3	Ti4	Ti5	Ti6	Rb ⁺
O1	3.06(8)	2.61(12)	3.56(52)		2.05(3)					2.88(4)
O2	2.40(8)			1.97(6) ^a						3.06(3)
O3				1.92(4)	1.95(8) ^c					
O3'					1.95(8) ^c					
O4				1.93(6) ^b			1.99(1)			
O5					1.93(3)	1.96(1)				
O6						1.98(1)	1.95(1)			
O6'						1.98(1)				
O7										
O8									1.99(1)	
Rb ⁺	2.62(8)	2.43(12)	3.23(52)					1.94(1)		

Numbers in parentheses are the uncertainties for the last one or two digits. Shown in the table are the distances between the adjacent atoms/ions.

^a Average of two distances of 1.94/2.00 ± 0.03 Å due to the two symmetry equivalent lateral positions of Ti1.

^b Average of two distances of 1.90/1.96 ± 0.03 Å due to the two symmetry equivalent lateral positions of Ti1.

^c Average of two distances of 1.90/2.01 ± 0.03 Å due to the two symmetry equivalent lateral positions of Ti2.

is significantly longer than a typical Ti–O bond in the bulk rutile crystal (1.98 Å). On the other hand, it is shorter than those reported by the DFT calculations (2.25–2.41 Å) [11,48–51] and photoelectron diffraction (PhD) measurement (2.21 ± 0.02 Å) [8] for the case of thin H₂O films adsorbed at the rutile (110)–UHV interface. The PhD measurement was carried out in UHV at ~ 200 K and it was believed that the amount of adsorbed water was no more than a single monolayer. No evidence of dissociation of water upon adsorption was observed in that experiment and the derived rutile surface relaxations with and without the adsorbed water were similar. Therefore, it was believed that the water associatively adsorbed at rutile (110) surface and the Ti–OH₂ interaction is fairly weak [8]. This agrees with the STM observation of adsorbed water molecules diffusing along *y*-direction ([001] direction) on top of Ti2 site, where the mobility of adsorbed water indicates a weak interaction with the surface Ti2 site [7] at low water coverage.

DFT calculations predicted that the Ti2–O1 bond length would be ~ 1.90 Å when water adsorbed dissociatively and >2.25 Å when adsorbed associatively [11]. The derived Ti2–O1 distance from the CTR result falls in between the two distances expected for molecular and dissociative adsorption. This might suggest a mixture of the two adsorbed species at the rutile–DIW interface, which is consistent with multi-site complexation (MUSIC) model calculations of the proton affinity of the oxygen at the TO site [18,52], which predicts mainly OH₂ at near-neutral pH, and a much higher proportion of surface OH[−] groups at this site at pH 12 to produce a negatively-charged surface.

We can ask if these data can offer further insight about whether associatively and dissociatively adsorbed water coexist at the rutile–DIW interface, i.e. with two distinct heights at the TO site, or if only one species, i.e. one height, is present. The best-fit model prefers a single height at the TO site to two heights, for which a vibration amplitude of $r_z = 0.1 \pm 0.1$ Å along *z*-direction is obtained if optimized. Given the vertical resolution of the measurements $z_{\text{res}} \sim p/Q_{z\text{max}} = 0.5$ Å, where $Q_{z\text{max}}$ is the maximum momentum transfer in the vertical direction, the data can be equally well-fitted with a two-height model that retains the observed rms width of this species, i.e. with relative displacements less than $r_z/0.55 = 0.18$ Å [36]. This is smaller than the expected difference (~ 0.35 Å) between the associatively and dissociatively adsorbed water molecule heights from DFT calculations, which suggests that even if two distinct TO heights coexist at the rutile (110)–DIW interface, the separation of the two may not be as large as those predicted by DFT calculations.

In comparing the CTR data to the previous work, it is important to note that the previous calculations/measurements were done at the low water coverage, i.e. less than or equal to 1 ML, while the present CTR data were obtained in contact with macroscopic water layer. Therefore the coverage of the adsorbed water appears to be the main reason for the different surface structures that are observed.

Similar effect has been observed before on the NaCl (100) surface exposed to water vapor, where structures of both the NaCl surface and the adsorbed water vary as the relative humidity changes [53].

A recent DFT calculation with ~ 2 ML of adsorbed water molecules above the rutile (110) surface showed the bond length of Ti–OH and Ti–OH₂ are 1.98 and 2.19 Å, respectively, when both associative and dissociative adsorption exist on the surface [54]. The displacement between the two heights (0.21 Å), is significantly smaller than those in the earlier calculation with less than 1 ML of adsorbed water molecules. A mixture of the two heights would be able to explain the CTR data as well as the single-height best-fit model.

At the rutile–RbCl solution interface, the Ti2–O1 distance is derived to be 2.05 ± 0.03 Å, which is significantly shorter than that at the rutile–DIW interface. It appears that the strengthening of the Ti2–O1 bond is due to the increased pH, resulting in a larger negative surface charge. In classical EDL models, the development of surface charge at elevated pH is associated with desorption of protons from the molecularly adsorbed water molecule in the TO site [55,56], resulting in a transition of the adsorbate species in the TO site from H₂O to OH[−]. The observed decrease in Ti2–O1 distance is consistent with this transition.

When the measured Ti2–O1 distance is a coherent average of the two distinct heights, it can be used to constrain the fraction of dissociatively adsorbed species. The difference of the average value between the solution conditions can be attributed to the fractional change of the two coexisting species, assuming the Ti–OH and Ti–OH₂ bond lengths are unaffected by changes in solution conditions. From this we estimate that $30 \pm 15\%$ of the TO sites are occupied by the dissociatively adsorbed water at the rutile–DIW interface, while $65 \pm 15\%$ are found at the rutile–RbCl solution interface. These numbers are within error equivalent to MUSIC model predictions that Ti–OH occupies $\sim 45\%$ of surface sites in the pH 5.6, 10^{-4} *m* RbCl electrolyte solution, and 75% in the pH 12, 1 *m* RbCl solution, as listed in Table 4. Therefore, the combination of CTR results, DFT calculations, and MUSIC model predictions strongly suggest the coexistence of associatively and dissociatively adsorbed water at the TO site, with the ratio between these states depending on solution conditions (primarily pH).

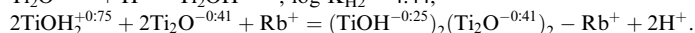
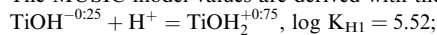
If the occupancy factors of O1 and O2 sites were fitted independently, larger-than-1 occupancy factors were obtained for both sites with improved fitting quality. But physically such model is questionable. There are a few possible scenarios where the nominal occupancy factors can be higher than one. One is the presence of protons that are not accounted for in the fitting by using the atomic form factor of an O atom for both O1 and O2 sites. Therefore the nominal occupancy factors might be larger if the O1/O2 sites were protonated (as OH[−] or H₂O). Attempts to use atomic form factor of O[−] and O^{2−} ions at the O1 and O2 sites

Table 4

Surface species fractions at the rutile (110)–aqueous solution interface by prediction from MUSIC model and estimation from CTR measurements

	Solution	pH	IS (<i>m</i>) ^b	TO ^a		BO ^a		Rb ⁺
				TiOH ^{-0.25}	TiOH ₂ ^{+0.75}	Ti ₂ O ^{-0.41}	Ti ₂ OH ^{+0.59}	
MUSIC	1	5.6	10 ⁻⁴ (RbCl)	0.44	0.56	0.90	0.10	0
	2	12	1 (RbCl)	0.76 ^c	0.24	0.98 ^c	0.03	0.17 ^d
CTR	DIW	~5.5	<10 ⁻⁵	0.30(15) ^e	0.70(15) ^e	–	–	–
	RbCl	12	1	0.65(15) ^e	0.35(15) ^e	–	–	0.40(10)

The MUSIC model values are derived with the following protonation constants and fractional charges: [23,25]



^a The sum of species at the TO sites is 1, so is that for BO sites.

^b IS is the ionic strength of the solution.

^c Values include ligands in the species $(\text{TiOH}^{-0.25})_2(\text{Ti}_2\text{O}^{-0.41})_2 - \text{Rb}^+$.

^d In MUSIC model, the adsorbed Rb⁺ species is $(\text{TiOH}^{-0.25})_2(\text{Ti}_2\text{O}^{-0.41})_2 - \text{Rb}^+$.

^e Values in the parentheses are the uncertainties for the last two digits.

failed to produce any significant difference. Another possibility is the exchange of the O atom by heavier atoms/ions (e.g., Cl⁻) due to previous exposure to Cl⁻ containing solutions. If this were true, we would expect that the occupancy factors of the O1 and O2 sites in the 1 *m* RbCl solution be different from the same surface in DIW due to the presence of Cl⁻ ions in the solution. However, no significant difference in the O1 and O2 occupancy factors were obtained from the fitting. Therefore, we believe that the high occupancy factors for the O1 and O2 sites are artifacts and that a more consistent way to interpret the data is obtained by linking the occupation factors of these two species with that of the underlying Ti2 and Ti1 sites.

In DIW, the distance between the O2 site and the adsorbed H₂O at site *A*₁ is 2.42 ± 0.05 Å, which is smaller than a typical O–O distance in bulk water [57]. It only changes slightly when the RbCl solution is introduced, with a bond length of 2.40 ± 0.08 Å. Such short O–O distance is similar to that observed on the RuO₂ (110)–water interface under the high applied potential (500 mV) [28], although our samples were not subjected to either external high potential or high pressure (under which condition ice X forms). Another possibility is the O–H⋯O hydrogen bond does not form along a straight line, e.g. for a hydrogen bond length of ~1.65 Å, the O–H⋯O bond angle would be ~30°. The component at site *A*₁ is needed to explain the CTR data although its physical origin is unclear. If it is an adsorbed water molecule, the short O–O distance leads to the suggestion of a strong interaction between the BO and adsorbed H₂O at the *A*₁ site, possibly sharing a proton in between the two oxygen atoms. Considering that the derived Ti1–O2 distance (1.95 ± 0.02 Å in DIW and 1.97 ± 0.06 Å in RbCl solution) is very close to a typical bulk rutile Ti–O bond length, bond valence theory would require the additional bond(s) to the BO atom be comparable to that in a typical Ti–O bond, ~0.6 v.u.. With a shared proton between O2 and *A*₁ site water offering ~0.5 v.u., the bond valence requirement for O2 oxygen is close to saturation.

When a water molecule adsorbs to the TO site dissociatively, a proton is transferred to a neighboring BO site to form a bridging hydroxyl (Ti₂–OH). According to the recent DFT calculations, the Ti₂–O and Ti₂–OH bond lengths are 1.89 and 1.99 Å, respectively, on this mixed adsorption surface [54]. Similar to the TO site, the small displacement here implies that the CTR measured Ti1–O2 distance could be explained by a coherent average of the two distinct distances. The measured Ti1–O2 distances show no significant difference at the two solution conditions, which suggests that the protonation statuses at the BO sites do not change significantly with changes in solution condition. This trend agrees well with the MUSIC predictions that 10% and ~3% the sites are protonated in DIW and in RbCl solution, respectively. Because of the small difference between the two Ti1–O2 distances and the relatively large uncertainties in the CTR measurements, it is hard to obtain useful values on the percentage of the BO sites which is protonated in DIW and RbCl solution.

Although the distance between the O1 site and the adsorbed H₂O at site *A*₃ (AW3) is also around 2.40 Å, the larger uncertainty in the lateral position of adsorbed H₂O at site *A*₃ makes the uncertainty in the distance >0.14 Å. It is therefore close to a typical hydrogen bond length.

Interpretation of the adsorbed Rb⁺ distribution is complicated because the CTR measurements are sensitive only to the total electron density. Rb⁺ ions and H₂O molecules are interchangeable at any of the model derived locations for Rb⁺ and three adsorbed waters. Directly comparing the laterally-averaged electron density profile as a function of the distance from the interface, as shown in Fig. 5, the higher interfacial electron density can be seen for the rutile–RbCl solution interface. If all of the adsorption sites are occupied exclusively by Rb⁺ ions, the total Rb⁺ coverage would be <1 ML, which is well below the theoretical full packed density (~2.3 ML) given the space available at the rutile–RbCl solution interface. This indicates that not all the sites are occupied by Rb⁺ ions. Some of them therefore must be water molecules. On the other hand, if

all the sites are occupied by water molecules, the coverage would be >4 ML to reach the derived electron density at the interface, which is also unrealistic. To account for the increase of the electron density, the Rb^+ ions are required to be present at the interface, primarily at the A_4 site, although we can not rule out the possibility of a very small amount of Rb^+ at the A_2 site, where the inter-atomic distance also agrees with the Rb-O bond length. The actual number density of Rb^+ ions and water molecules at the interface can be estimated based on the constraint derived from the sizes of the Rb^+ ion and water molecule combined with the measured total electron density. The estimated total Rb^+ ion coverage is $\sim 0.4 \pm 0.1$ ML and the water coverage is ~ 1.9 ML. A second way to estimate the Rb coverage is to subtract the two derived profiles and associate the increased electron density with the substitution of Rb^+ for a water molecule [58]. This procedure also gives a Rb^+ coverage of $\sim 0.4 \pm 0.1$ ML.

The MUSIC model predicted Rb^+ coverage in the pH 12 RbCl solution is 0.17 ML, which is smaller than the CTR derived one. This discrepancy could be partially due to the large uncertainty in the CTR coverage estimation. The present CTR measurements only probe the total electron density of the interfacial system, as detailed in the discussion above. Although it has sensitivity to changes in the interfacial structure, this technique has no specific ability to probe the element specific distribution of a given cation, as was done with previous XSW measurements. Consequently, it is difficult for the CTR method to precisely reveal the occupancy of each of the species in a complex system, such as the rutile–electrolyte interface, where there is more than one type of species occupying the same or similar positions. Resonant anomalous X-ray scattering measurement [59] should be able to reduce this uncertainty and provide more precise information concerning the ion distributions at this and similar interfaces.

In order to discuss the likely bond lengths for adsorbed Rb^+ , each of the surface atoms and/or adsorbate are considered to have up to four equivalent sites due to the surface symmetry. All the possible configurations are explored and the more likely scenarios are highlighted based on the Rb-O distance. The distance between the adsorbed Rb^+ ion and the adjacent O1, O2, TO, and BO sites are all close to the Rb-O bond length in aqueous solution (~ 2.60 Å) [60], as listed in Table 3. This confirms that mono-valent cations, such as Rb^+ , can specifically adsorb at the rutile (110)–water interface as inner-sphere species. Given the locations and the distance between the adsorbed Rb^+ ion and the AW2 water molecule, the AW2 water is unlikely to be one of the Rb^+ hydration shell waters. It is more likely an independently adsorbed species coexisting at the interface, i.e. the Rb^+ ion and AW2 water molecule should be located laterally in different surface 2D unit cells.

The adsorbed Rb^+ ions are found to primarily occupy the A_4 sites, which is also the primary adsorption sites of Sr^{2+} and Y^{3+} ions based on previous XSW measurements [24]. Since water molecules occupy the same site at the ru-

tile–DIW interface, it is reasonable to believe that the tetradentate site is the lowest potential site on the (110) surface thus the primary position to fill when an adsorbate comes into contact with the surface. The alkali cations, including Rb^+ , are normally thought of as the indifferent “background” electrolyte ions that are only present in the diffuse double layer as fully-hydrated cations. The measurements here directly prove that picture is incorrect. Like multivalent ions, Rb^+ ions also adsorb specifically as inner-sphere species at the interface. The primary difference is a much weaker thermodynamic driving force (i.e. weaker binding constant) due to the reduced charge. This is seen when comparing with Sr^{2+} , which yielded a surface coverage of ~ 0.4 ML at solution condition of 10^{-4} M concentration and pH 10.7, whereas Rb^+ ions achieved this level of adsorption only at 1 M concentration and pH 12. Therefore when present in the solution at the same time, the Rb^+ is in competition for sorption at the inner-sphere sites with multivalent cations, as discussed previously [27].

6. Summary

CTR measurements have been used to probe the detailed structure of the rutile (110)–aqueous solution interface. The crystal surface structure in 1 M RbCl solution at pH 12 is similar to that in DIW, albeit with smaller interfacial relaxations, especially for Ti atoms in the RbCl solution. Both BO and TO sites are fully occupied in aqueous solutions. Above the BO and TO layer, an additional water layer is observed with well-defined vertical and lateral molecular locations. No further water layering is observed beyond this layer.

At the rutile (110)–DIW interface, the Ti atoms below the BO row relax outwards and the Ti atoms below the TO row relax inwards, with their relaxation amplitudes decreasing from 0.05 Å at the surface to ~ 0.01 Å at the fourth Ti-layers. The Ti2–O1 distance is observed to be 2.13 ± 0.03 Å, suggesting the water adsorbs primarily molecularly at the TO site. There are three water adsorption locations at a similar height above the TO site, around the A_4 , A_3 , and A_1 sites, respectively.

At rutile (110)– RbCl solution interface at pH 12, the relaxations of the Ti atoms are similar to those in DIW, except with smaller amplitudes. The Ti2–O1 distance is observed to be 2.05 ± 0.03 Å, suggesting that dissociatively adsorbed water, i.e. OH^- , as the dominant species at the TO site, as predicted from proton-affinity calculations [18,52]. The adsorbed water layer structure is perturbed by Rb^+ ions, which primarily replaces the adsorbed water molecules at the A_4 (tetradentate) site. While the adsorbate at the A_1 site has minimal change between DIW and RbCl solution, the adsorbate at the A_3 site is removed and another component shows up at the A_2 site. A water molecule is also observed next to the adsorbed Rb^+ ion further away from the surface, probably associated with the hydration shell of Rb^+ . The coverage of adsorbed Rb^+ is estimated to be ~ 0.4 ML at this condition.

The distances of adsorbed Rb^+ ions to surface oxygens in the BO and TO sites are similar to the average bond length of hydrated Rb^+ in bulk aqueous solution. This indicates that four of the hydrating water molecules are replaced by four surface oxygens when Rb^+ sorbs at the tetradentate (A_4) site, to form an inner-sphere species. This observation provides definitive proof that ‘background electrolyte’ ions compete directly with multivalent ions for sorption at inner-sphere sites, though the sorption affinities of the multivalent ions are much stronger, due to the increased cation charge. This competition for sorption at inner sphere sites provides a partial explanation for the often-observed ionic strength dependence of multivalent cation adsorption on metal oxide surfaces.

Acknowledgements

We would like to thank Dr. Lawrence Anovitz for the treatments of the rutile crystal. We would also like to thank Drs. Peter Lee, Yuegang Zhang, and Suresh Narayanan for their assistance in beamline setup. This work was performed primarily at beamline 1-BM at the Advanced Photon Source, with preliminary measurements performed at 12-BM, 11-ID-D and 12-ID-D. This work was supported by U.S. Department of Energy, Office of Science, Office of Basic Energy Sciences, Chemical Sciences, Geosciences, and Biosciences Division, and through its support for the Advanced Photon Source, under Contract DE-AC02-06CH11357.

References

- [1] P.C. Hiemenz, R. Rajagopalan, *Principles of Colloid and Surface Chemistry*, Marcel Dekker, New York, 1997.
- [2] G.E. Brown et al., *Chem. Rev.* 99 (1999) 77.
- [3] U. Diebold, *Surf. Sci. Rep.* 48 (2003) 53.
- [4] M.A. Henderson, *Surf. Sci. Rep.* 46 (2002) 5.
- [5] A. Fujishima, K. Honda, *Nature* 238 (1972) 37.
- [6] R. Wang, K. Hashimoto, A. Fujishima, M. Chikuni, E. Kojima, A. Kitamura, M. Shimohigoshi, T. Watanabe, *Nature* 388 (1997) 431.
- [7] S. Wendt, J. Matthiesen, R. Schaub, E.K. Vestergaard, E. Laegsgaard, F. Besenbacher, B. Hammer, *Phys. Rev. Lett.* 96 (2006) 066107.
- [8] F. Allegretti, S. O'Brien, M. Polcik, D.I. Sayago, D.P. Woodruff, *Phys. Rev. Lett.* 95 (2005) 226104.
- [9] M.A. Henderson, *Langmuir* 12 (1996) 5093.
- [10] L.A. Harris, A.A. Quong, *Phys. Rev. Lett.* 93 (2004) 086105.
- [11] A.V. Bandura, D.G. Sykes, V. Shapovalov, T.N. Truong, J.D. Kubicki, R.A. Evarestov, *J. Phys. Chem. B* 108 (2004) 7844.
- [12] C.J. Zhang, P.J.D. Lindan, *J. Chem. Phys.* 118 (2003) 4620.
- [13] R.E. Tanner, M.R. Castell, G.A.D. Briggs, *Surf. Sci.* 412–413 (1998) 672.
- [14] G. Charlton et al., *Phys. Rev. Lett.* 78 (1997) 495.
- [15] R. Lindsay, A. Wander, A. Ernst, B. Montanari, G. Thornton, N.M. Harrison, *Phys. Rev. Lett.* 94 (2005) 246102.
- [16] P.A. O'Day, C.J. Chisholm-Brause, S.N. Towle, G.A. Parks, J. Brown, E. Gordon, *Geochim. Cosmochim. Acta* 60 (1996) 2515.
- [17] S.N. Towle, G.E. Brown, G.A. Parks, *J. Colloid Interf. Sci.* 217 (1999) 299.
- [18] M.L. Machesky, D.J. Wesolowski, D.A. Palmer, M.K. Ridley, *J. Colloid Interf. Sci.* 239 (2001) 314.
- [19] M.V. Fedkin, X.Y.Y. Zhou, J.D. Kubicki, A.V. Bandura, S.N. Lvov, M.L. Machesky, D.J. Wesolowski, *Langmuir* 19 (2003) 3797.
- [20] M. Predota, A.V. Bandura, P.T. Cummings, J.D. Kubicki, D.J. Wesolowski, A.A. Chialvo, M.L. Machesky, *J. Phys. Chem. B* 108 (2004) 12049.
- [21] M. Predota, Z. Zhang, P. Fenter, D.J. Wesolowski, P.T. Cummings, *J. Phys. Chem. B* 108 (2004) 12061.
- [22] M. Predota, L. Vlcek, *J. Phys. Chem. B* (Submitted for publication) Erratum to *J. Phys. Chem. B* 108 (2004) 12049; *J. Phys. Chem. B* 108 (2004) 12061.
- [23] Z. Zhang et al., *Langmuir* 20 (2004) 4954.
- [24] Z. Zhang, P. Fenter, L. Cheng, N.C. Sturchio, M.J. Bedzyk, M.L. Machesky, D.J. Wesolowski, *Surf. Sci.* 554 (2004) L95.
- [25] M.K. Ridley, M.L. Machesky, D.J. Wesolowski, D.A. Palmer, *Geochim. Cosmochim. Acta* 69 (2005) 63.
- [26] Z. Zhang et al., *Geochim. Cosmochim. Acta* 70 (2006) 4039.
- [27] Z. Zhang, P. Fenter, L. Cheng, N.C. Sturchio, M.J. Bedzyk, M.L. Machesky, L.M. Anovitz, D.J. Wesolowski, *J. Colloid Interf. Sci.* 295 (2006) 50.
- [28] Y.S. Chu, T.E. Lister, W.G. Cullen, H. You, Z. Nagy, *Phys. Rev. Lett.* 86 (2001) 3364.
- [29] S.C. Abrahams, J.L. Bernstein, *J. Chem. Phys.* 55 (1971) 3206.
- [30] I.K. Robinson, *Phys. Rev. B: Condens. Matter* 33 (1986) 3830.
- [31] S.A. De Vries, P. Goettkindt, S.L. Bennett, W.J. Huisman, M.J. Zwanenburg, D.M. Smilgies, J.J. De Yoreo, W.J.P. Van Enckevort, P. Bennema, E. Vlieg, *Phys. Rev. Lett.* 80 (1998) 2229.
- [32] P.J. Eng, T.P. Trainor, G.E. Brown, G.A. Waychunas, M. Newville, S.R. Sutton, M.L. Rivers, *Science* 288 (2000) 1029.
- [33] L. Cheng, P. Fenter, K.L. Nagy, M.L. Schlegel, N.C. Sturchio, *Phys. Rev. Lett.* 8715 (2001).
- [34] P. Fenter, in: P. Fenter, M.L. Rivers, N.C. Sturchio, S.R. Sutton (Eds.), *Applications of Synchrotron Radiation in Low-Temperature Geochemistry and Environmental Sciences*, Washington, 2002, pp. 149.
- [35] M.F. Reedijk, J. Arsic, F.F.A. Hollander, S.A.d. Vries, E. Vlieg, *Phys. Rev. Lett.* 90 (2003) 066103.
- [36] P. Fenter, N.C. Sturchio, *Prog. Surf. Sci.* 77 (2004) 171.
- [37] I.K. Robinson, D.J. Tweet, *Rep. Prog. Phys.* 55 (1992) 599.
- [38] Y. Bard, *Nonlinear Parameter Estimation*, Academic Press, New York, 1974.
- [39] N.R. Draper, H.S. Smith, *Applied Regression Analysis*, John Wiley & Sons, New York, 1981.
- [40] J.C. Lang, G. Srajer, J. Wang, P.L. Lee, *Rev. Sci. Instrum.* 70 (1999) 4457.
- [41] P. Fenter, L. Cheng, S. Rihs, M. Machesky, M.J. Bedzyk, N.C. Sturchio, *J. Colloid Interf. Sci.* 225 (2000) 154.
- [42] I.M. Brookes, C.A. Muryn, G. Thornton, *Phys. Rev. Lett.* 87 (2001) 266103.
- [43] C. Zhang, P.J.D. Lindan, *J. Chem. Phys.* 119 (2003) 9183.
- [44] O.M. Magnussen, B.M. Ocko, M.J. Regan, K. Penanen, P.S. Pershan, M. Deutsch, *Phys. Rev. Lett.* 74 (1995) 4444.
- [45] A. Braslau, P.S. Pershan, G. Swislow, B.M. Ocko, J. Alsnielsen, *Phys. Rev. A* 38 (1988) 2457.
- [46] C.J. Howard, T.M. Sabine, F. Dickson, *Acta Crystallogr., Sect. B: Struct. Sci* 47 (1991) 462.
- [47] S.J. Thompson, S.P. Lewis, *Phys. Rev. B: Condens. Matter* 73 (2006) 073403.
- [48] M. Casarin, C. Maccato, A. Vittadini, *J. Phys. Chem. B* 102 (1998) 10745.
- [49] E.V. Stefanovich, T.N. Truong, *Chem. Phys. Lett.* 299 (1999) 623.
- [50] M. Menetrey, A. Markovits, C. Minot, *Surf. Sci.* 524 (2003) 49.
- [51] C. Zhang, P.J.D. Lindan, *J. Chem. Phys.* 121 (2004) 3811.
- [52] J.P. Fitts, M.L. Machesky, D.J. Wesolowski, X. Shang, J.D. Kubicki, G.W. Flynn, T.F. Heinz, K.B. Eisenthal, *Chem. Phys. Lett.* 411 (2005) 399.
- [53] J. Arsic, D.M. Kaminski, N. Radenovic, P. Poodt, W.S. Graswinckel, H.M. Cuppen, E. Vlieg, *J. Chem. Phys.* 120 (2004) 9720.
- [54] J.D. Kubicki, A.V. Bandura, J.O. Sofo, *Abstr. Pap. Am. Chem. Soc.* 232 (2006) COLL 476.

- [55] T. Hiemstra, W.H. Van Riemsdijk, G.H. Bolt, J. Colloid Interf. Sci. 133 (1989) 91.
- [56] M.L. Machesky, D.J. Wesolowski, D.A. Palmer, K. Ichiro-Hayashi, J. Colloid Interf. Sci. 200 (1998) 298.
- [57] P.A. Thiel, T.E. Madey, Surf. Sci. Rep. 7 (1987) 211.
- [58] M.L. Schlegel, K.L. Nagy, P. Fenter, L. Cheng, N.C. Sturchio, S.D. Jacobsen, Geochim. Cosmochim. Acta 70 (2006) 3549.
- [59] C. Park, P.A. Fenter, N.C. Sturchio, J.R. Regalbuto, Phys. Rev. Lett. 94 (2005) 076104.
- [60] Y. Marcus, Ion Properties, Marcel Dekker, New York, 1997.